Optical Materials 60 (2016) 422–430

Contents lists available at ScienceDirect

Optical Materials

journal homepage: www.elsevier.com/locate/optmat

Multilayer design of hybrid phosphor film for application in LEDs

Tuğrul Güner [a], Devrim Köseoğlu [b], Mustafa M. Demir [a, *]

[a] Department of Material Science and Engineering, Izmir Institute of Technology, Izmir, Turkey
[b] Vestel Electronics, LED Lighting R&D Department, O.S.B., 45030, Manisa, Turkey

ARTICLE INFO

Article history:
Received 29 May 2016
Received in revised form
4 July 2016
Accepted 24 August 2016
Available online 2 September 2016

Keywords:
Phosphor converted w-LED
PDMS
Remote phosphor
Spray coating
White light
YAG:Ce^{3+}

ABSTRACT

Crosslinked polydimethylsiloxane (PDMS) composite coatings containing luminescent micrometer-sized yellow $Y_3Al_5O_{12}:Ce^{3+}$ (YAG:Ce^{3+}) particles were prepared by spraying for potential applications in solid-state lighting. Blue light was down converted by phosphor particles to produce white light, yet poor color properties of YAG:Ce^{3+} stemmed from a deficiency of red. When nitride-based red phosphor was simply blended into the system, the electrostatic interaction of negatively charged YAG:Ce^{3+} and positively charged red phosphor particles caused remarkable clustering and heterogeneity in particle dispersion. Consequently, the light is dominantly blue and shifted to cold white. In other case, phosphor particles were sprayed onto the diffused polycarbonate substrate in stacked layers. Coatings with >80% inorganic content by mass with a thickness of 60 μm were subjected to thermal crosslinking, which the presence of the phosphor particles obstructed, presumably due to the hindrance of large phosphor particles in the diffusion of PDMS precursors. The coating of YAG:Ce^{3+} first followed by red phosphor in stacked layers produced better light output and color properties than the coating obtained by spraying the mixture at once. Monte Carlo simulation validated the hypothesis.

1. Introduction

Since lighting is responsible for nearly 20% of electricity consumption worldwide [1], the invention of light-emitting diodes (LED) has been deemed a breakthrough in minimizing global energy consumption [2]. LED lighting has also prompted the production of a wide range of lighting applications, including in white light, as a promising alternative to incandescent and fluorescent lamps [3,4]. In that context, the combination of red, green, and blue LEDs has emerged as a straightforward solution for fabricating white light. However, given the different requirements of individual LEDs—for instance, their independent driving currents and the degradation-related characteristics of materials employed—mixing different colors in coherence necessarily involves a complex system of integration [2,3].

As an alternative, blue light can be down converted with yellow phosphor [2,3,5,6]. Polymer-based composite films containing yellow garnet particles provide flexible composite films for direct or remote applications with blue LEDs. A part of the incident light passes through the film with virtually no attenuation or backscattering, while some of the primary light is absorbed and converted by the phosphors to secondary light. The combination of incident light and secondary light passing through the film forms white light. To that end, various polymer–phosphor particle systems have been employed for down conversion [7–9], including CeF_3:(Tb^{3+}, Dy^{3+}, Eu^{3+}) [10], YVO_4:(Eu^{3+}) [11], GYAG [12], YAG:(Ce^{+3}, Gd^{3+}) [13], YAG:(Ce^{+3}) [8,14–16], Zn_2SiO_4:(Mn^{2+}, Eu^{3+}) [17], $BaIn_6Y_2O_{13}$:(Yb^{3+}, Tm^{3+}, Er^{3+}) [18] particles dispersed in poly(-methyl methacrylate), Na_2SO_4 [19] and $BaAl_xO_y$:(Eu^{2+}, Dy^{3+}) [20] in low-density polyethylene, YAG:Ce^{+3} in polydimethylsiloxane (PDMS) [21,22], and YBO_3:(Eu^{2+}) [23] and YGG:(Tb^{3+}) [24] in a polyvinylpyrrolidone matrix. In any case, the goal is a stable white light with a high color rendering index (CRI) and high luminous efficacy as well as a light color that is stable and almost independent of the charged current. However, that attractive optical feature is governed entirely by the quality of the material components and the internal microstructure of the composite coating [25,26].

Widely used for white-LED applications due to its high conversion efficiency, better energy-saving aspects than incandescent and fluorescent lighting, and low cost, cerium-doped yttrium aluminum garnet (YAG:Ce^{3+}) has been used as yellow phosphor

Abbreviations: PDMS, Polydimethylsiloxane; CIE, Commission Internationale de l'éclairage; CRI, Color Rendering Index; CCT, Correlated Color Temperature; FTIR, Fourier Transform Infrared Spectroscopy; YAG:Ce^{+3}, Cerium doped Yttrium Aluminum Garnet; $Sr_2Si_5N_8$:Eu^{+2}, Europium doped Strontium Silicon Nitride.

* Corresponding author.
E-mail address: mdemir@iyte.edu.tr (M.M. Demir).

http://dx.doi.org/10.1016/j.optmat.2016.08.023
0925-3467/

[27]. However, YAG:Ce^{3+} possess serious shortcomings, including thermal quenching [28], a low CRI due to red emission deficiency [29]. Whereas remote phosphor setup has been used to prevent thermal quenching [30], additional red phosphor—that is, europium-doped strontium silicon nitride ($Sr_2Si_5N_8$:Eu^{2+})—has been used to improve overall CRI and the resulting color properties. By comparison, PDMS—a transparent binder and polymeric carrier employed in spraying—has a rotationally flexible Si–O bond that allows an unusually high degree of chain flexibility [31], as well as greater bonding energy (452 kJ/mol) than common vinyl polymers with C–C bonds (347 kJ/mol) [32]. Considering the sustained exposure of light-converting film to highly energetic blue light, PDMS also offers greater UV resistance than other vinyl polymers.

PDMS is an inexpensive hydrophobic polymer that can be coated as thin films on solid surfaces. Ability to wet nearly any substrate surface, appropriate viscoelastic behavior, and cross-linkable nature make PDMS suitable coating material for various processes. In the structural development of coating, the interaction of material components—for instance, the interaction of phosphor particles with polymer precursors and other ingredients—and the spatial arrangement of phosphor particles are critical parameters. In this study, the interaction of YAG:Ce^{3+} and PDMS precursors and red phosphor were examined in detail. YAG:Ce^{3+} and red phosphor particles were sprayed either as a random mixture in a single layer or consecutively as two distinct stacked layers from the PDMS and hexane solution, which achieved the multilayer buildup of coating. Crosslinking was monitored by vibrational spectroscopy, both in the absence and presence of phosphor particles, and the morphology of the coatings was examined by both optical and scanning electron microscopy techniques. The surface charge of the particles was studied in terms of the zeta potential of dynamic light scattering, whereas the optical performance of coatings prepared by the two strategies was compared in terms of correlated color temperature (CCT), CRI, and efficacy.

2. Experimental

2.1. Materials and methods

Phosphor powders YAG:Ce^{3+} and $Sr_2Si_5N_8$:Eu^{2+} (HB-4155H and HB-640, Zhuhai Hanbo Trading Co., Ltd., Guangdong, China) were used as received. PDMS (SYLGARD 184 Kit, Dow Corning, Midland, MI, USA) was used as a polymer matrix for film formation. Due to high viscosity of PDMS, hexane (>95%, Sigma–Aldrich, St. Louis, MO, USA) was used to thin the PDMS powder solutions. The diffraction pattern of the phosphor powders was recorded with an X-ray diffractometer (X'Pert Pro, Philips, Eindhoven, the Netherlands), and the photoluminescence (PL) spectrum was recorded on a fluorescence spectrophotometer (Cary Eclipse, Agilent, Palo Alto, CA, USA). Fourier transform infrared spectroscopy (FTIR; Spectrum 100, PerkinElmer, Shelton, CT, USA) was used to characterize and track changes in the kinetic behavior of bonds, and scanning electron microscopy (SEM; Quanta 250, FEI, Hillsboro, OR, USA) was used to determine particle morphology. The dispersion of powders in PDMS was observed with an optical microscope (BX 53, Olympus, Tokyo, Japan), while spectra of the resulting emissions were recorded by spectrometer (USB2000+, Ocean Optics Inc., Dunedin, FL, USA). Color coordinates and flux were obtained by an integrating sphere (ISP-50-80-R, Ocean Optics Inc.) connected with the USB2000 + spectrometer via premium fiber cable.

2.2. Preparing the phosphor composite film

Spraying is a coating technique used to make homogeneous films on a given substrate. By atomizing a solution or dispersion using high air pressure, the process is uniquely suited for dispersions consisting of heavy, large guest particles in host polymer solutions. In this study, phosphor particles with a density of approximately 4.6 g cm^{-3} were sprayed in the form of PDMS–phosphor dispersion thinned by hexane to polycarbonate (PC) diffuser substrates (Scheme 1). Following the standard process, powder was added into a test tube, and the composition of YAG:Ce^{3+} and red phosphor was fixed to 5:1 by mass ratio. PDMS precursors, i.e. a vinyl-ended PDMS oligomers and the curing agent were dropped in a 10:1 mixing ratio with respect to mass into a test tube. Next, hexane was added to reduce viscosity, the dispersion was mixed in a magnetic stirrer and poured into the hopper of a spray gun (400 W, 1–2 bar pressure), and spray coating was performed onto a set of PC substrate 7–10 s. The resulting composite coatings were approximately 60 μm thick; one side of the substrate was smooth and reflective, whereas another surface—the diffuser side—was rough. Phosphor was sprayed onto the diffuser side because rough surfaces can hold the phosphor coating. The samples were left in open air overnight so that the hexane could fully evaporate, after which they were cured at 100 °C for 2 h in an oven.

2.3. Optical measurement

With a diode emitting a monochromatic blue light at 478 nm, two types of measurement techniques were applied: direct and remote measurements. In the former, the PDMS–phosphor coating on the PC substrate was placed directly onto the blue LED chip so that the composite coating were placed directly over the chip. In the latter, a fixed distance (3 cm) was maintained between the film and LED surface in a black chamber (Scheme 2). Altogether, the system was run with a 0.35 mA input current.

The quality of color is crucial in determining color rendition. One measure of color rendition is the ability of a light source to produce the colors of various objects, which can be quantified by CRI. The best possible rendition shows a CRI of 100, whereas the poorest shows a CRI of 0. Typically, a CRI >80 is preferred in various applications. Another parameter that describes the quality of light is CCT, or the measure of the blackbody temperature needed to radiate a hue comparable to that of the related light source. In general, CCT >5000 K is called bluish white (cool) and 2500 < CCT < 5000 K yellowish white. Since white light is perceived by the human eye with particular precision, luminous efficacy (LEF) is used to define whether the efficiency of an overall spectrum falls within the region matching eye sensitivity [33]. LEF is

$$LEF = 683lm/W \frac{\int v(\lambda)\varnothing(\lambda)d\lambda}{\int \varnothing(\lambda)d\lambda} \quad (1)$$

in which $v(\lambda)$ is the luminosity function representing human perception normalized to unity at a wavelength of 555 nm due to eye sensitivity and $\varnothing(\lambda)$ is the spectral power distribution per wavelength. Given the definition of $v(\lambda)$, the inner product between the luminosity function and spectral power distribution should be 380–780 nm with 5-nm intervals.

3. Results and discussion

3.1. YAG:Ce^{3+} and red phosphor particles

Fig. 1 shows the morphological and structural characterization of the phosphor particles. Fig. 1a and 1b presents SEM images of the YAG:Ce^{3+} and red phosphor powders, respectively; YAG:Ce^{3+} had a nearly monodisperse polyhedral shape, whereas $Sr_2Si_5N_8$:Eu^{2+}

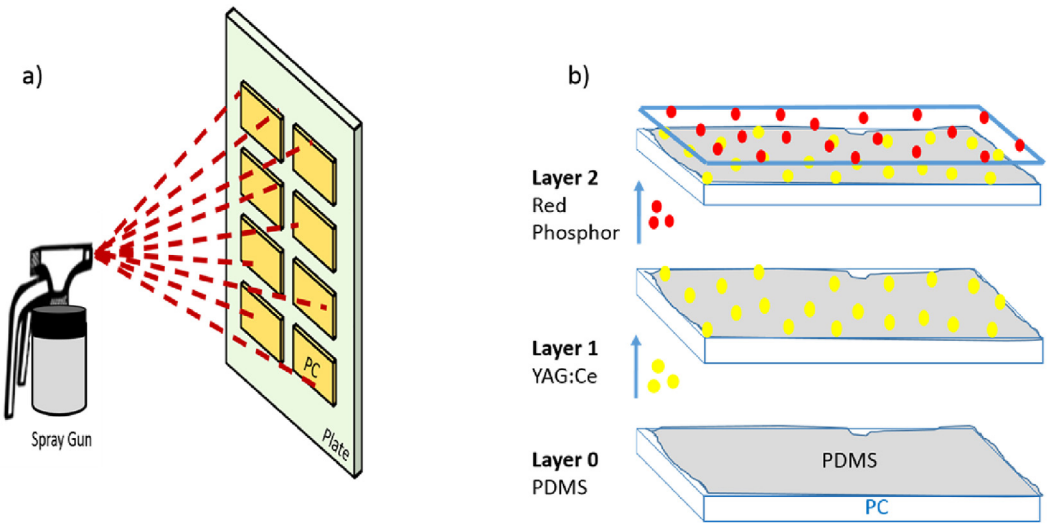

Scheme 1. Schematic illustration of the spray coating process. Panel a shows the spray of PDMS/Phosphor solution towards PC substrates that are placed carefully on a plate. Panel b is the demonstration of coating strategy followed during spraying representing the stacking layer.

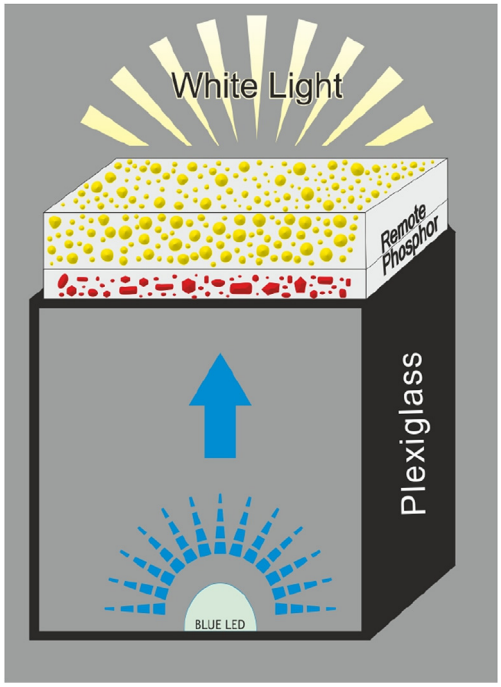

Scheme 2. Schematic view remote phosphor configuration.

powder had a rather polydispersed shape that changed from polyhedral to rod-like crystals. This difference was also verified by particle size distributions obtained by the statistical treatment of particles using ImageJ in Fig. 1c and 1d [34]. Although both powders demonstrated a close mean diameter of nearly 10 μm, $Sr_2Si_5N_8:Eu^{2+}$ had a broader distribution than YAG:Ce^{3+} that extended the tail of the distribution to 60 μm in diameter. Fig. 1e shows the X-ray diffraction pattern of both yellow and red phosphor powders. Reflections were indexed with the crystallographic data of host materials YAG and $Sr_2Si_5N_8$ with Joint Committee on Powder Diffraction Standards (card nos. 01-082-0575 and 01-085-0101, respectively). Fig. 1f illustrates the PL spectrum of the phosphors at room temperature. YAG:Ce^{3+} showed two absorption bands centered at 340 nm and 460 nm. Those bands can be related to 4f → 5d absorption transitions where 5d states are splitted due to the crystal field effect of the doped Ce^{3+} ions. The broad emission band of YAG:Ce^{3+} centered at 550 nm is the backward emissive transition from the lowest 5d states to 4f states collected at the 478 nm wavelength. By contrast, red phosphor has a single broad excitation band at 440 nm collected at the 620 nm wavelength, and a narrower emission band at 620 nm collected at the 478 nm wavelength.

3.2. Structural development of the composite coatings

Many wet processing approaches—for example, casting, spin coating, and those with doctor blades—were used to obtain PDMS composite homogeneous in terms of both particle dispersion and film thickness. To obtain homogeneous, well-dispersed phosphor particles, the primary requirement of the approaches is to form stable colloid dispersion. The sedimentation of the phosphor colloids is inevitable, since the density of the particles is far greater than that of the polymer and solvent. This density mismatch renders solution-based processing nearly impossible, as well as deteriorates the homogeneity of the coating. Although stabilizing the particles using various surfactants, including cetyltrimethyl ammonium bromide, sodium dodecyl sulfate, and Triton X-100, was studied, none of the surfactants could stabilize the large particles in the polymer solution. Spray coating appears to be the most convenient approach for forming composite coating with large, heavy particles along with a minor amount of polymeric carrier. Moreover, unlike with other wet processing methods, the high particle content can be loaded into the polymeric system.

Two different spraying strategies were employed. In the first, the PDMS/YAG:Ce^{3+} dispersion was sprayed as the first layer, upon which PDMS/red phosphor was sprayed as the second (Scheme 1). In the second strategy, YAG:Ce^{3+} and red phosphor were mixed with PDMS solution and sprayed on PC substrate at once. In both spraying strategies, pristine PDMS (i.e., without particles) was initially sprayed onto the PC substrate as the so-called zeroth layer. Since particles are much heavier than the surrounding PDMS matrix, they have a strong tendency toward sedimentation through the substrate in the long run, even though the matrix is crosslinked. Such engulfment may cause a segregation of the phosphor particles

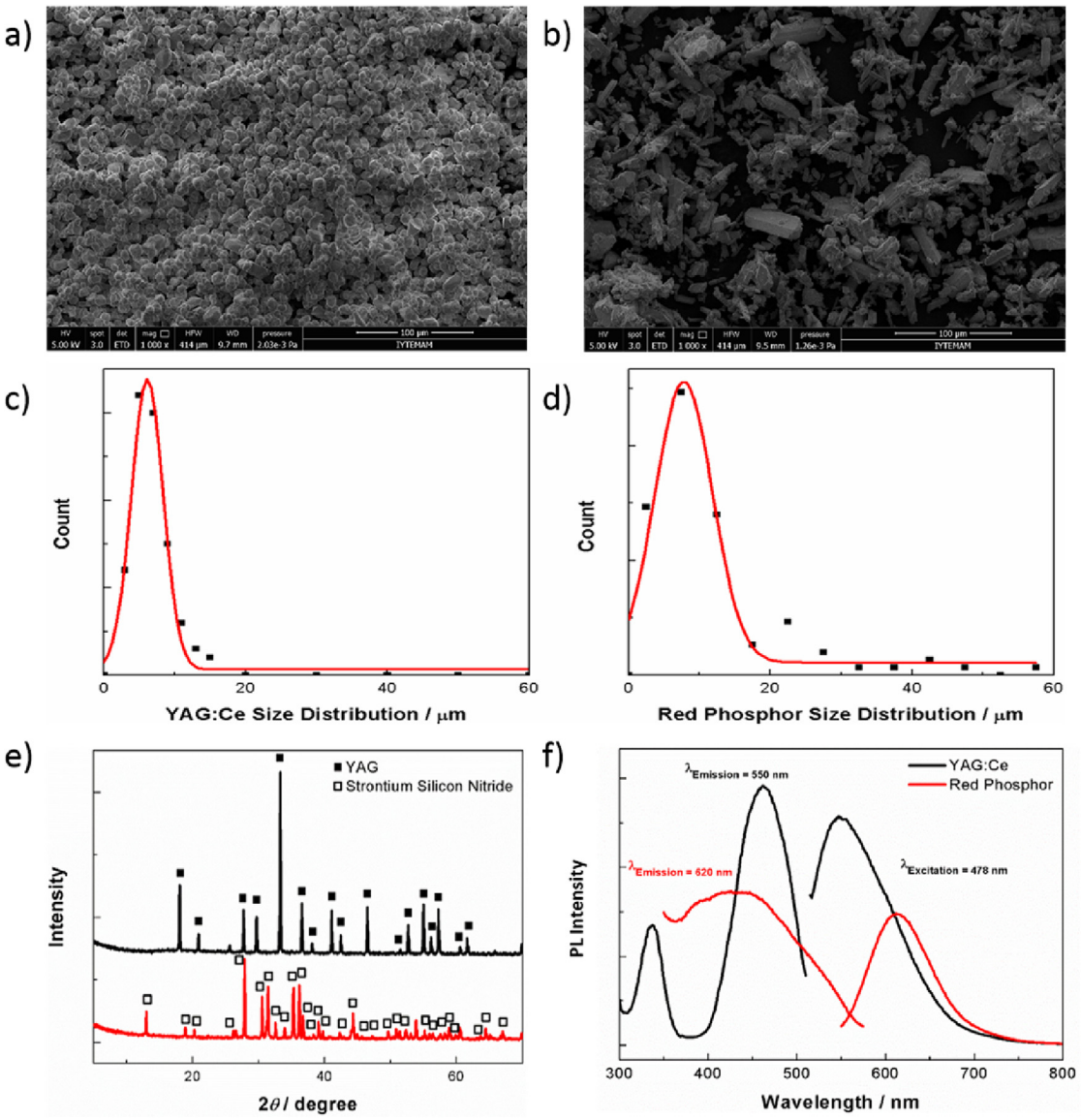

Fig. 1. SEM images of a) YAG:Ce^{3+}, and b) red phosphor powders. Size distribution of these related phosphors, c) YAG:Ce^{3+}, and d) red phosphor are also calculated. Panel e is the XRD pattern of phosphor powders, and panel f is PL spectrum of the phosphor powders. Excitation spectrum was recorded with emission wavelength at 550 nm, and emission spectrum was recorded with the excitation wavelength at 478 nm which is same as the blue LED for YAG:Ce^{3+} (black line). For the red phosphor (red line), excitation spectrum was recorded at emission wavelength at 620 nm. Emission spectrum details are same with the YAG:Ce^{3+}. (For interpretation of the references to colour in this figure legend, the reader is referred to the web version of this article.)

at the interface of the PC substrate and PDMS matrix. The homogeneous dispersion of the particles in coating eventually worsens particle dispersion and precludes optical stability [35–37].

Crosslinking PDMS occurs via the hydrosilylation of a difunctional vinyl-ended oligomers and four functional groups of the crosslinker methylhydrosiloxane. A Pt catalyst under ambient atmospheric conditions catalyzes the crosslinking reaction, thereby achieving a network throughout the coating volume. During crosslinking, Si–CH=CH_2 bonds of the oligomer interact with Si–H bonds of the curing agent. As a result, Si–CH_2–CH_2–Si chains form intricately until the curing agent is consumed. At the same time, the disappearance of the vibrational signal of Si–H at 2163 cm^{-1} hints at the progress of crosslinking, the reactions of which were monitored for 2 h. Fig. 2a presents attenuated total reflection mode of the corresponding FTIR spectra of the crosslinking process registered at 4000–400 cm^{-1}. With time, the intensity of this vibrational signal with respect to time disappears, thereby indicating the progress of the crosslinking reaction.

The same process was performed in the presence of 10% and 40% phosphors by mass. Fig. 2b and c shows the first and second derivative of the intensity of the signal in the presence of 10% and 40% particles, respectively; the first refers to the absorbance signal's rate of change (i.e., speed), whereas the second presents the acceleration of the process. PDMS alone has the highest initial change rate, which is followed by an exponential decrease with respect to time. However, in the presence of phosphor, the initial change rate becomes remarkably reduced. The reduction becomes more remarkable as the phosphor content increases. For instance, at 30 min, the initial rate of the neat PDMS was 85%, yet 79% and 52% for the 10% and 40% particle content, respectively. Similarly, the acceleration of the process reduced by the initial Si–H content; whereas it was 85% for PDMS alone and decreased to 58% for PDMS coating with 10%

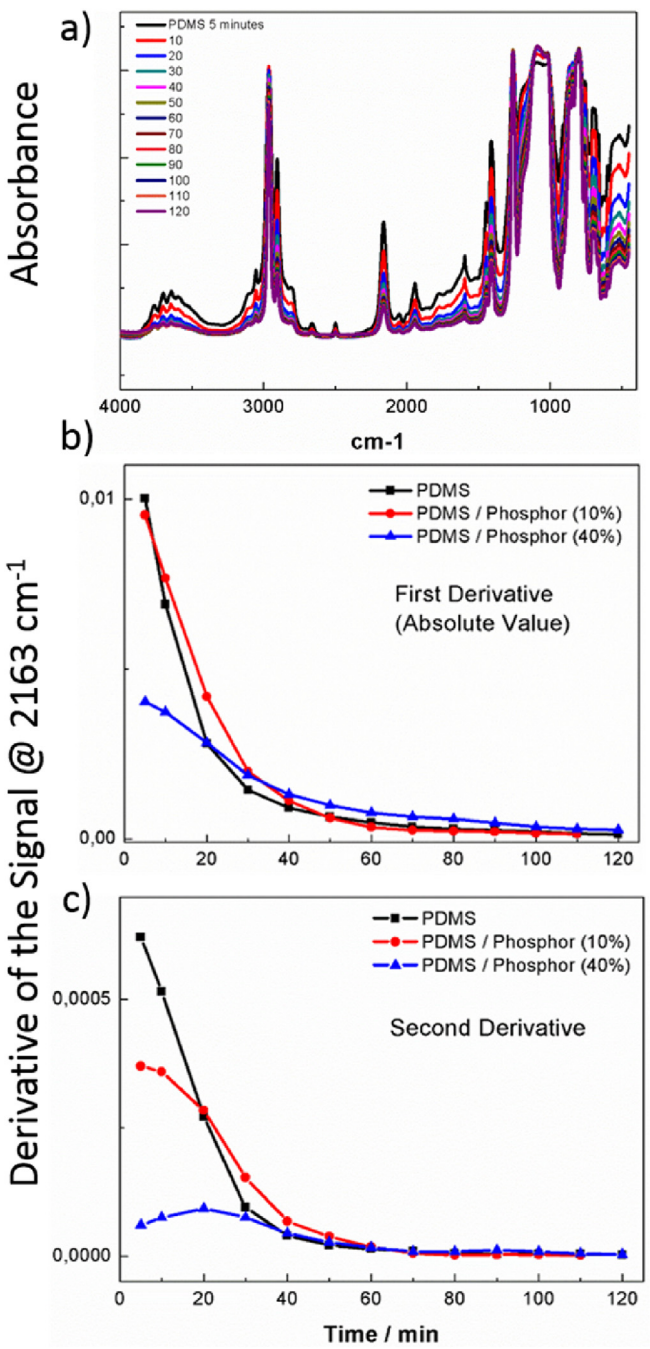

Fig. 2. FTIR spectrum of cross-linking process. Panel a presents the change of FTIR signals with respect to time was shown for neat PDMS. In panel b, and c, effect of the different phosphor contents on the FTIR signals during cross-linking were analyzed by focusing on first and second derivatives of the Si–H signal at the 2163 cm^{-1} respectively.

phosphor particles, there was nearly no acceleration for the PDMS–phosphor 40% sample. Clearly, crosslinking is remarkably hindered in the presence of garnet particles, yet nevertheless had been completed in 2 h. The reason for such results could be the hindrance of the diffusion of precursors in the presence of large phosphor particles. Alternatively, such hindrance could stem from the interaction of the particle surfaces with precursors of PDMS in the *in situ* crosslinking process. For confirmation, the particles were treated with the difunctional vinyl-ended oligomer methylhydrosiloxane and crosslinking counterparts, albeit separately. The diffuse reflectance infrared Fourier transform of the particles was registered after isolating the garnet particles via sedimentation and rigorous washing. The spectra of the particles showed strong $Si–CH_3$ signals that stretched at approximately 2900 cm^{-1}. The presence of the signals in both spectra could suggest a remarkable interaction between particle surface and both PDMS and the curing agent (Figure S2).

Fig. 3a shows the optical microscope image of composite coating prepared by spraying YAG:Ce^{3+} and red phosphor consecutively on a neat PDMS layer. Displayed with differently colored arrows, phosphor particles seemed homogeneously dispersed over a 50×50-μm^2 area. A cross-section of the composite films prepared by consecutive spraying was examined by SEM, and the electron micrograph in Fig. 3b verifies three distinct layers. The zeroth layer is the first layer on the substrate, above which phosphor particles are evident; a dashed line guiding the eye indicates that yellow particles are sandwiched between the zeroth PDMS and red phosphor/PDMS layers. Assuming the homogeneous dispersion of particles throughout coating, $>10^6$ phosphor particles were expected per cm^2 of coating.

By contrast, the YAG:Ce^{3+} and red phosphor mixture in Fig. 3c is clearly heterogeneous, implying that mixing two different phosphor particles causes the formation of large clusters of the both yellow and red phosphor particles, as well as develops cracks and particle-lean regions in coating. To gain further insight into the reason for such heterogeneity, YAG:Ce^{3+} and red phosphor particles were dispersed into the PDMS–hexane solution, albeit separately. The surface charge of the particles was measured by the zeta potential mode of dynamic light scattering (Fig. 3d); for instance, YAG:Ce^{3+} is an oxide particle in nature, and its charge is negative at nearly −10 mV. The origin of the negative charge could be the partial dissociation of the surface hydroxyl group inevitable with any oxide on a particle surface. At the same time, red phosphor showed positive potential at nearly +5 mV. When both YAG:Ce^{3+} and red phosphor were mixed in the PDMS–hexane solution during spraying, a Coulombic attraction occurred between the negatively charged yellow and positively charged red particles such that large pseudo-clusters formed in the dispersion and thus in the resulting coating.

3.3. The optical performance of composite coatings

Fig. 4a and b shows the PL spectra of the composite coatings obtained by remote and direct measurement strategies, respectively. Regardless of phosphor type employed, an unidentified weak emission signal was obtained at 610 nm in all spectra; this signal might have originated from an impurity in the phosphor system or from the ore in which mineral phosphor particles were achieved, if not both. An intensely sharp signal at 478 nm was attributed to the primary blue light from the blue LED, whereas the broad signal at 550 nm with relatively lower intensity referred to the emission of YAG:Ce^{3+} garnet particles. The 4f → 5d transition of the Ce^{+3} ions in the garnet structure absorbed the incoming blue light, while its corresponding emission appeared in the yellow region [38]. Because blue and yellow are complimentary colors, their combination resulted in white light emission.

The chief difference between the direct and remote sets of spectra is the ratio of signals in blue and yellow regions. Signals obtained from the direct measurement were greater than with remote measurement. Since the distance of the phosphor layer and the blue LED was closer, yellow phosphor particles were more intensively exposed to blue light. As a result, the emission unsurprisingly appeared greater with direct measurement.

The quality of white light can be determined from the ratio of blue and yellow signals in the spectrum [39]. Since YAG:Ce^{3+} is

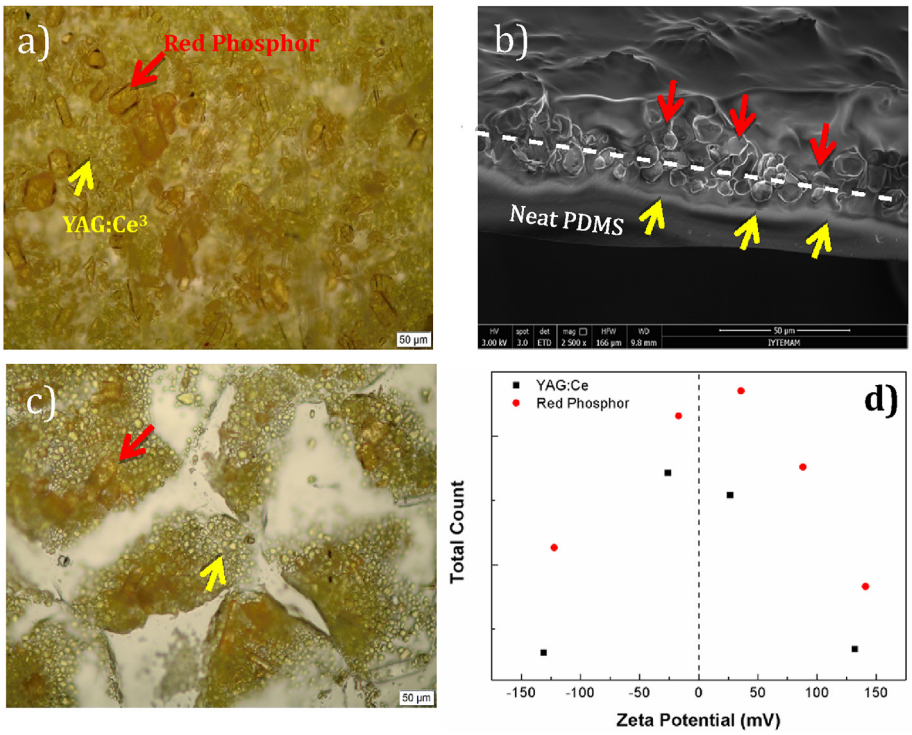

Fig. 3. Optical microscope image of a) is the optical microscope image of the stacking. Panel b is the SEM image of stacking sample but focused on the cross section under 2500× magnification and c) is the optical microscope image of the mixture as single layer sample. Red and yellow arrows show the red phosphor and YAG:Ce^{3+} particle(s), respectively. Panel d is the surface charge of the phosphor particles in PDMS/hexane solution by zeta potential mode of dynamic light scattering. (For interpretation of the references to colour in this figure legend, the reader is referred to the web version of this article.)

deficient in the red region, $Sr_2Si_5N_8$:Eu^{2+} can be added to improve quantity-related color properties (e.g., CCT and CRI). Upon incorporating red phosphor, the overall emission shifted from 550 to 605 nm; however, the arrangement of the phosphor with respect to the incoming blue light strongly influenced the color properties of the white light; for instance, the coating prepared by spraying YAG:Ce^{3+} and red phosphors consecutively as stacked layers presented far greater emission over the yellow–red region than spraying the mixture of the phosphors once in a single layer, even though they had the same amount and composition of phosphors. For comparison, spectrum of commercial products are given in Figure S3. Fig. 4c and d shows the absolute spectral flux obtained from remote and direct measurements, respectively. Clearly, the mixture has intense blue light, which reduces the contribution of phosphors in developing white light. The inadequacy of the mixture in all optical properties emerged simply due to the presence of large empty spaces across the film, as shown in the optical microscope images (Fig. 3c). Blue LED escapes from empty regions without any interaction with the phosphors. At the same time, since those spaces exist less in coating prepared in stacked layers of multiple phosphors using consecutive spraying, a homogeneous dispersion of phosphor particles in two layers over coating can be achieved. Fig. 5a shows photographic images of white light produced as obtained by down converting blue LED by coatings via stacking layers and the random mixture of phosphor particles; the former displayed much better as a white light source in terms of human perception, thereby confirming the microscopy and spectroscopy results above. It should be noted that in the stacked layer arrangement, the sequence of phosphor layers is critical. In general, spectrum is dominated by the phosphor layer, whichever is placed as a primary layer over the blue LED. The incoming blue light first interacts with the primary layer without any particular loss, but reflection. On the other hand, the second layer only interacts with the remaining of the incident light, which passes without interacting with the phosphors in the primary layer. This mechanism leads to an inefficiency for the second layer in terms of blue light interaction. Therefore, choosing the appropriate phosphor for related layers becomes a useful tool for tuning the overall spectrum. In our particular case, red phosphor was chosen as primary layer to overcome red deficiency of overall spectrum dominated by YAG:Ce due to its very high concentration compared to red phosphor. Herewith, blue LED first contacts with red phosphor, whose emission at approximately 620 nm cannot excite yellow YAG:Ce^{3+}. Otherwise, blue LED's first contact with the YAG:Ce^{3+} emission from those yellow phosphors is absorbed by the red phosphor, which renders the use of red phosphor inefficient (Fig. 5b).

Table 1 shows CRI, CCT, and efficacy values. The coating prepared with YAG:Ce^{3+} only showed 4500 K, 61 CRI, and 253 lm $watt^{-1}$ luminous efficacy. YAG:Ce^{3+} in PDMS thus seems adequate in fabricating cool, white light, yet with limited efficacy. However, coating prepared with the mixture of YAG:Ce^{3+} and red phosphor in spraying was inadequate and even worse than coating prepared with YAG:Ce^{3+} along. The clustering of phosphor particles resulted in large empty regions dominated by blue light such that CRI and CCT could not be successfully registered in remote measurements. The coating consisting of phosphor particles in two distinct layers improved both color properties and light output; CCT, CRI, and luminous efficacy were 2900 K, 68, and 264 lm $watt^{-1}$, respectively, and color space coordinates x (CIE_x) and y (CIE_y) were between 0.3 and 0.4. These values were also assessed for direct measurement, which generally provided higher values for both CRI and CCT. Note that those values can be adjusted by simply arranging the distance between the phosphor layer and the light source.

In real-time applications, PDMS–phosphor coatings are exposed

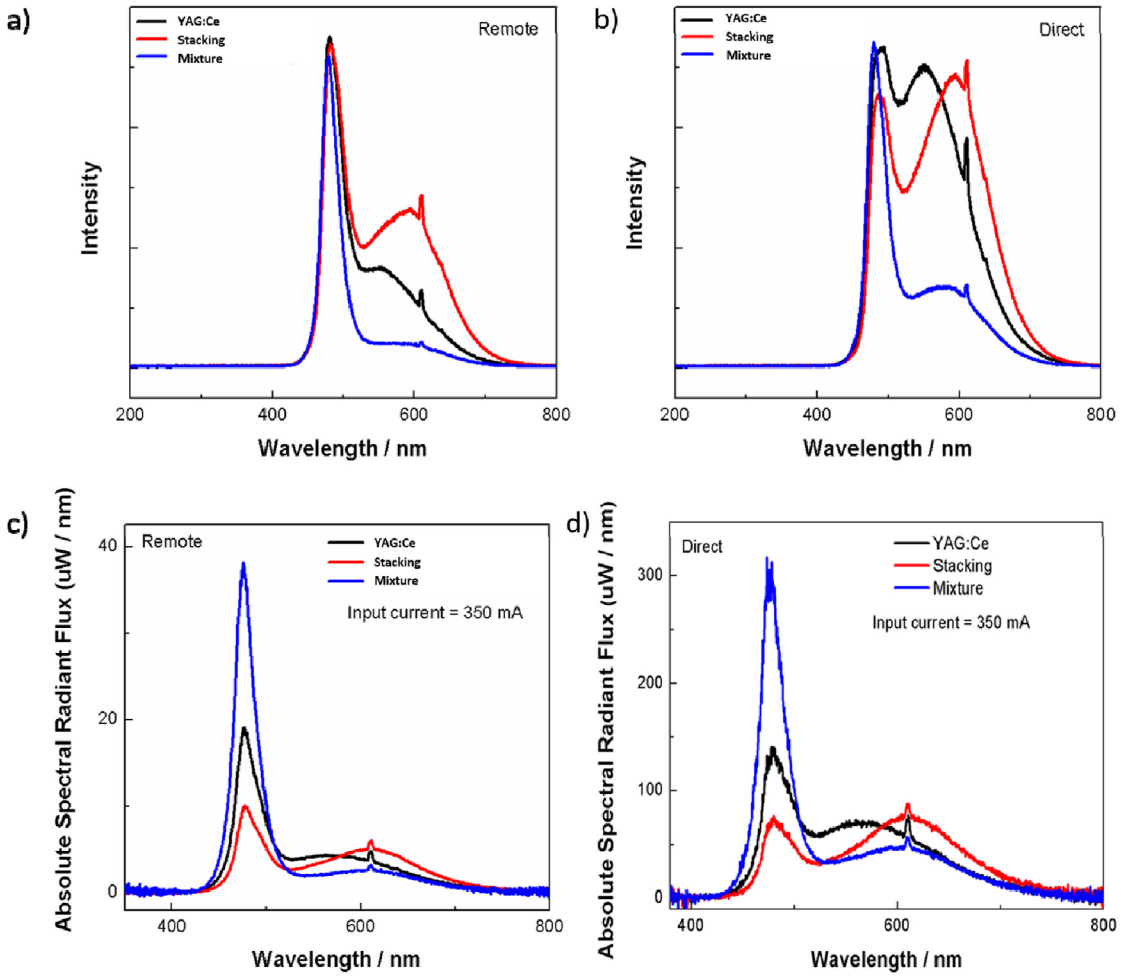

Fig. 4. Spectrum of PDMS/phosphor coated PC substrates. In panel a remote phosphor measurement was done at 3 cm away from the blue LED source and in panel b direct phosphor measurement was done without having any distance between sample and blue LED source. Irradiance of samples under blue LED illumination having 0.35 A input current collected by using the c) remote and d) direct measurement.

to blue light for a long time. Such exposure can eventually trigger secondary reactions and cause undesirable consequences—for instance, the degradation of PDMS that may have adverse effects on the film's optical stability. When blue LED continuously illuminated a piece of representative coating of stacked layers for 4 weeks, periodically registered spectra remained unchanged, thereby indicating that the coating was stable under blue light, at least in the range of conditions employed (i.e., time and atmospheric humidity) in this study (Figure S4).

3.4. Simulation

The arrangement of phosphor particles in the PDMS matrix was simulated using the Monte Carlo approach developed with the programming language Python [40]; program codes appear in the Supporting Information. The spectra were simulated between the 400 and 750 nm wavelengths, considering stacking and random mixture separately. Assuming monolayer coverage of the substrate by phosphor particles, the intensity of the resulting light was determined by the algorithm for each wavelength. When light impinged the phosphor coating, the intensity was attenuated via two mechanisms—namely, reemission (due to absorption) and scattering—the probability of each of which is calculated by a partition function consisting of Gaussian functions representing all possible emissions—that is, blue LED as transmission and both yellow and red as re-emissions—by following the formulas [41].

$$I_{tm} = I_0 \exp\left(-4ln2 \frac{(\lambda - \lambda_{tm})^2}{FWHM_{tm}^2} \right) \quad (2)$$

$$I_{rm}(y|r) = I_{rm}(y|r)\ \exp\left(-4ln2 \frac{(\lambda - \lambda_{rm})^2}{FWHM_{rm}^2} \right) \quad (3)$$

in which I_0, and I_{rm}(y|r) are the peak intensities of blue LED, YAG:Ce^{3+}, and red phosphors in the experimentally measured spectra, respectively, λ is the wavelength, and λ_{tm}, λ_{rm_y} and λ_{rm_r} are the corresponding wavelengths of the peak intensities of blue LED, YAG:Ce^{3+}, and red phosphor. Similarly, $FWHM_{tm}$, $FWHM_{rm\_y}$, and $FWHM_{rm\_r}$ are at full width at half of the maximum of related blue LED, YAG:Ce^{3+}, and red phosphor. The total possible event is thus

$$I_{total} = I_{tm} + I_{rm\_y} + I_{rm\_r} \quad (4)$$

in which I_{rm_y} and I_{rm_r} are the corresponding spectrum intensity of YAG:Ce^{3+} and red phosphor, respectively. As a result, the probability of each event in the corresponding wavelength in the spectrum can be defined as:

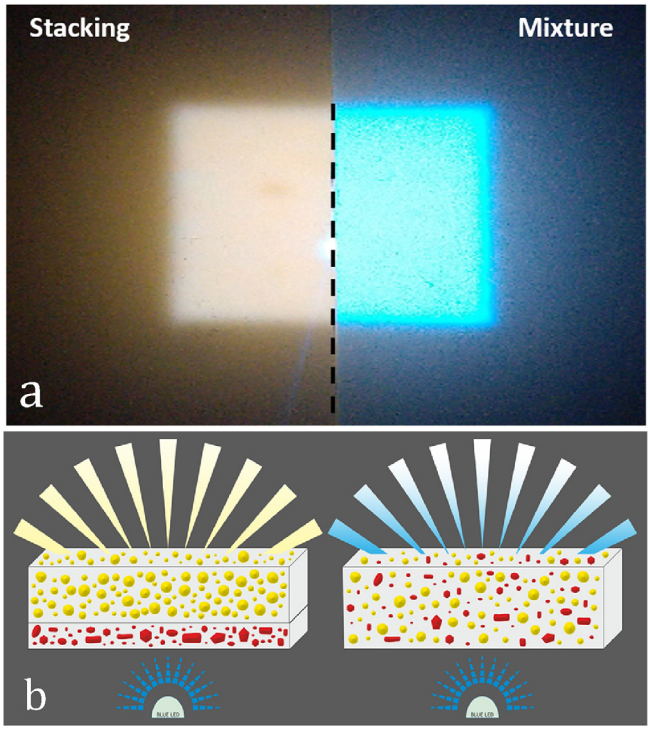

Fig. 5. a) Comparison of illumination of the coatings prepared by the mixture and stacked layers of the phosphor particles b) cartoon demonstration of the interaction of blue light with coatings prepared with two strategies. The one prepared by consecutive spraying provides adequate quality of warm white light.

In stacking phosphor particles, incoming light first interacts with the red phosphor with a probability of 27%. YAG:Ce^{3+} is assumed to interact with light based on the 3.7:1 volumetric ratio of YAG:Ce^{3+} and red phosphor. Blue light will be either transmitted or absorbed by red phosphor, thereby prompting an emission. The YAG:Ce^{+3} layer of the sample interacts with blue light either directly, with a probability of 73%, or indirectly after scattered from the red phosphor. Following the same strategy, incoming blue light is either transmitted or absorbed by YAG:Ce^{3+} and causes a yellow emission. In the random mixture of the phosphor particles, the total empty region of the image of the optical microscope in Fig. 3a was first calculated by using ImageJ; the result was 40%. Incoming blue light was then directly transmitted with 40% probability. In the case of interaction, again due to the 3.7:1 volumetric ratio, incoming light hit the red phosphor with 22% and the YAG:Ce^{3+} with 78% probability since they are at the same level. In any case, every step of the interaction, the algorithm compares probabilities, then determines the intensity whether it goes with Eq. (2) or Eq. (3) 3000 times at each wavelength, and takes the average of the set of determinations. Regardless, transmission or reemission occurred according to the probabilities defined in Eqs. (5)–(7) for the corresponding wavelengths. Fig. 6 shows the results of simulating both remote and direct spectra; simulation shows the superiority of stacking layers over using the random mixture. In that sense, the results of simulation agree with the experimental results [42].

4. Conclusions

In this study, we investigated the fabrication of PDMS-based phosphor coating with yellow YAG:Ce^{3+} and red phosphor by spraying. The mixture of PDMS and phosphor particles were sprayed on a PC substrate, and the resulting coating was subjected to crosslinking at 100 °C. The phosphor particles with micrometer-sized diameters hindered, yet did not entirely obstruct the completion of the crosslinking process. Although red phosphor was integrated into the system, electrostatic interaction existed between YAG:Ce^{3+} and red phosphors, thereby causing the clustering of phosphor particles. As a result of clustering, cracks appeared in the coating, blue light dominated, and the light become cold white. Spraying yellow and red phosphor particles consecutively in stacked layers improved optical features compared to coating prepared by spraying the mixture as a single layer at once. The highest light output was obtained when the longer wavelength of red phosphor was placed on the YAG:Ce^{3+} as the second layer over PC substrate. This method was highly versatile in obtaining coating

Table 1
CIE color coordinates, color chromaticities CRI, CCT, and luminous efficacy of the coatings to both remote and direct phosphor configurations.

Sample	CIE_x		CIE_y		CRI		CCT (K)		LEF (lm/W)
	Remote	Direct	Remote	Direct	Remote	Direct	Remote	Direct	Remote
YAG:Ce^{3+}	0.3	0.4	0.3	0.4	61 ± 1.0	72 ± 1.0	8620 ± 200	4500 ± 50	253
Stacking	0.4	0.4	0.4	0.4	68 ± 1.5	82 ± 1.0	4300 ± 90	2900 ± 100	264
Mixture	[a]	0.3	[a]	0.3	[a]	54 ± 1.0	[a]	8000 ± 100	165

[a] No meaningful results were obtained from the measurement.

$$p_{tm} = \frac{I_{tm}}{I_{total}} \quad (5)$$

$$p_{rm\_y} = \frac{I_{rm\_y}}{I_{total}} \quad (6)$$

$$p_{rm\_r} = \frac{I_{rm\_r}}{I_{total}} \quad (7)$$

in which p_m, p_{rm_y}, and p_{rm_r} are for the blue LED, YAG:Ce^{3+}, and red phosphor, respectively. Peak intensities were determined by using Fig. 4a and b, while peak intensity wavelength and FWHM parameters were calculated by using the PL spectrum in Fig. 1f. Parameters are shown in Table 2.

Table 2
Peak intensity, peak wavelength and FWHM values of both remote and direct case used in the simulation.

Strategy	Peak intensity			Peak intensity wavelength			FWHM		
	I_{tm}	I_{rm_y}	I_{r_r}	λ_{tm}	λ_{rm_y}	λ_{rm_r}	$FWHM_{tm}$	$FWHM_{rm\_y}$	$FWHM_{rm\_r}$
Remote	884	373	355	478	550	620	30	129	82
Direct	1055	952	935	478	550	620	30	129	82

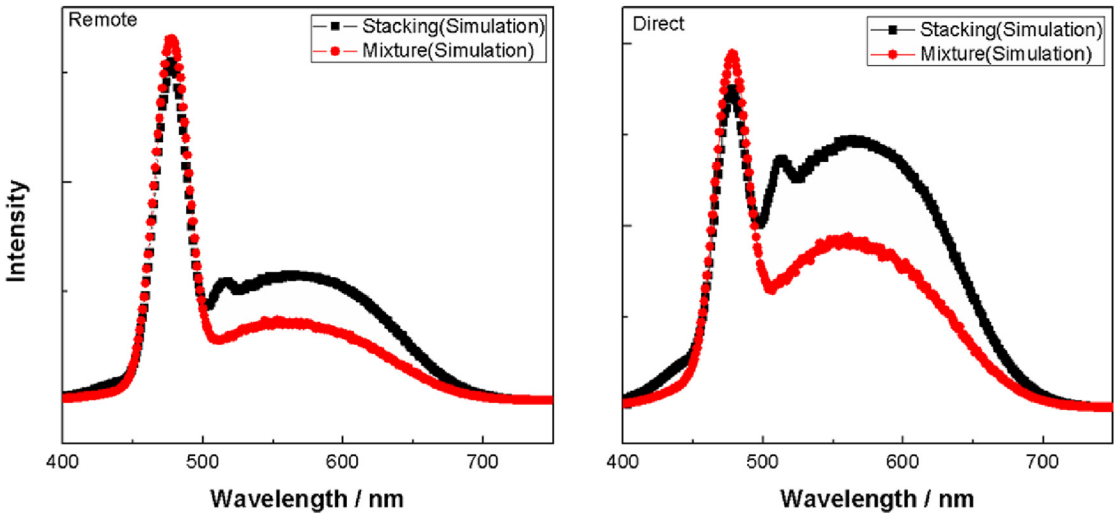

Fig. 6. Remote and direct spectrum obtained by simulation of stacking and mixture arrangement of phosphor particles in the PDMS coating.

materials on a large scale in a brief processing time and suitable in potential applications in both direct and remote solid-state lighting.

Author contributions

The manuscript was written through contributions of all authors. All authors have given approval to the final version of the manuscript.

Funding sources

This work was supported by "Outstanding Young Investigator" grant of the Turkish Academy of Sciences [TÜBA-GEBİP 2013]; and The Scientific and Technological Council of Turkey [TUBITAK Teydeb 1501 3150192].

Acknowledgments

The authors thank Center for Material Research of the Izmir Institute of Technology for microscopy work and C. Varlıklı for her critical reading of the manuscript.

Appendix A. Supplementary data

Supplementary data related to this article can be found at http://dx.doi.org/10.1016/j.optmat.2016.08.023.

References

[1] P. Waide, S. Tanishima, Light's Labour's Lost: Policies for Energy-efficient Lighting, OECD Publishing, 2006.
[2] K. Shinde, S. Dhoble, Crit. Rev. Solid State Mater. Sci. 39 (2014) 459–479.
[3] S. Ye, F. Xiao, Y. Pan, Y. Ma, Q. Zhang, Mater. Sci. Eng. R Rep. 71 (2010) 1–34.
[4] S. Tan, X. Sun, H. Demir, S. DenBaars, Photonics J. IEEE 4 (2012) 613–619.
[5] C.C. Lin, R.-S. Liu, J. Phys. Chem. Lett. 2 (2011) 1268–1277.
[6] N.C. George, K.A. Denault, R. Seshadri, Annu. Rev. Mater. Res. 43 (2013) 481–501.
[7] N. Narendran, Y. Gu, J. Freyssinier-Nova, Y. Zhu, Phys. Status Solidi (a) 202 (2005) R60–R62.
[8] S.C. Allen, A.J. Steckl, Appl. Phys. Lett. 92 (2008) 143309.
[9] Y.H. Song, G.S. Han, E.K. Ji, M.-J. Lee, Y.L. Song, M.K. Jung, B.W. Jeong, H.S. Jung, D.-H. Yoon, J. Mater. Chem. C 3 (2015) 6148–6152.
[10] F.N. Sayed, V. Grover, K. Dubey, V. Sudarsan, A. Tyagi, J. colloid interface Sci. 353 (2011) 445–453.
[11] D. Hreniak, J. Doskocz, P. GŁuchowski, R. Lisiecki, W. Stręk, N. Vu, D. Loc, T. Anh, M. Bettinelli, A. Speghini, J. luminescence 131 (2011) 473–476.
[12] D. Bera, S. Maslov, L. Qian, J.S. Yoo, P.H. Holloway, J. Disp. Technol. 6 (2010) 645–651.
[13] V. Tucureanu, A. Matei, I. Mihalache, M. Danila, M. Popescu, B. Bita, J. Mater. Sci. 50 (2015) 1883–1890.
[14] M.L. Saladino, A. Zanotto, D. Chillura Martino, A. Spinella, G. Nasillo, E. Caponetti, Langmuir 26 (2010) 13442–13449.
[15] M.L. Saladino, D. Chillura Martino, M.A. Floriano, D. Hreniak, L. Marciniak, W. Strek, E. Caponetti, J. Phys. Chem. C 118 (2014) 9107–9113.
[16] J. Oliva, E. De la Rosa, L. Diaz-Torres, A. Zakhidov, Phys. Status Solidi (a) 211 (2014) 651–655.
[17] L. Đačanin, S.R. Lukić, D.M. Petrović, Ž. Antić, R. Krsmanović, M. Marinović-Cincović, M.D. Dramićanin, J. Mater. Eng. Perform. 21 (2012) 1509–1513.
[18] J. Zhang, Y. Yang, C. Mi, Y. Liu, F. Yu, X. Li, Y. Mai, Dalton Trans. 44 (2015) 1093–1101.
[19] J. Zhang, A.Z.M.S. Rahman, Y. Li, J. Yang, B. Zhao, E. Lu, P. Zhang, X. Cao, R. Yu, B. Wang, Opt. Mater. 36 (2013) 471–475.
[20] D.B. Bem, H.C. Swart, A.S. Luyt, F.B. Dejene, J. Appl. Polym. Sci. 121 (2011) 243–252.
[21] d.A. Esteves, J. Brokken-Zijp, J. Laven, G. de With, Prog. Org. Coat. 68 (2010) 12–18.
[22] d.A. Esteves, J. Brokken-Zijp, J. Laven, H. Huinink, N. Reuvers, M. Van, G. de With, Polymer 51 (2010) 136–145.
[23] P.-O. Bussière, J. Peyroux, G. Chadeyron, S. Therias, Polym. Degrad. Stab. 98 (2013) 2411–2418.
[24] A. Potdevin, G. Chadeyron, S. Therias, R. Mahiou, Langmuir 28 (2012) 13526–13535.
[25] M.M. Demir, P. Castignolles, Ü. Akbey, G. Wegner, Macromolecules 40 (2007) 4190–4198.
[26] M.M. Demir, M. Memesa, P. Castignolles, G. Wegner, Macromol. Rapid Commun. 27 (2006) 763–770.
[27] Y. Pan, M. Wu, Q. Su, J. Phys. Chem. Solids 65 (2004) 845–850.
[28] V. Bachmann, C. Ronda, A. Meijerink, Chem. Mater. 21 (2009) 2077–2084.
[29] C.C. Lin, A. Meijerink, R.-S. Liu, J. Phys. Chem. Lett. 7 (2016) 495–503.
[30] Y. Shuai, N.T. Tran, J.P. You, F.G. Shi, Phosphor size dependence of lumen efficiency and spatial CCT uniformity for typical white LED emitters, in: Electronic Components and Technology Conference (ECTC), 2012, pp. 2025–2028. IEEE 62nd, IEEE2012.
[31] M.M. Demir, Y.Z. Menceloglu, B. Erman, Polymer 46 (2005) 4127–4134.
[32] S. Zumdahl, S. Zumdahl, Belmont, CA: Brooks/Cole, p. 374.
[33] T. Erdem, S. Nizamoglu, H.V. Demir, Opt. Express 20 (2012) 3275–3295.
[34] C.A. Schneider, W.S. Rasband, K.W. Eliceiri, Nat. Methods 9 (2012) 671–675.
[35] D. Rimai, L. DeMejo, Annu. Rev. Mater. Sci. 26 (1996) 21–41.
[36] D. Rimai, L. Demejo, J. Chen, R. Bowen, T. Mourey, J. Adhes. 62 (1997) 151–168.
[37] D. Rimai, D. Schaefer, R. Bowen, D. Quesnel, Langmuir 18 (2002) 4592–4597.
[38] M.M. Demir, G. Wegner, Macromol. Mater. Eng. 297 (2012) 838–863.
[39] N.T. Tran, J.P. You, F.G. Shi, Light. Technol. J. 27 (2009) 5145–5150.
[40] J.D. Hunter, Comput. Sci. Eng. 9 (2007) 90–95.
[41] X. Shen, D.-F. Zhang, X.-W. Fan, G.-S. Hu, X.-B. Bian, L. Yang, J. Mater. Sci. Mater. Electron. 27 (2016) 976–981.
[42] Y. Zhu, N. Narendran, Jpn. J. Appl. Phys. 49 (2010) 100203.